

## Retrieving vertical profiles of water-cloud droplet effective radius: Algorithm modification and preliminary application

Fu-Lung Chang and Zhanqing Li<sup>1</sup>

Earth System Science Interdisciplinary Center, University of Maryland, College Park, Maryland, USA

Received 24 June 2003; revised 20 September 2003; accepted 29 September 2003; published 18 December 2003.

[1] *Chang and Li* [2002] proposed a new cloud microphysics retrieval technique that can estimate the vertical profile of droplet effective radius (DER) for water clouds using multispectral near-infrared (NIR) measurements. The underlying principle of the retrieval technique is that radiance measurements at distinct multi-NIR wavelengths possess different penetration depths inside the cloud and this conveys certain information on the DER vertical profile (DVP). However, this information is insufficient to retrieve any shape of DVP and thus a linear DVP was assumed. In this study, three DVPs are examined: (1) as in *Chang and Li* [2002], a linear DVP proportional to the in-cloud optical depth, (2) a linear DVP proportional to the height within the cloud, and (3) a DVP where the liquid water content (LWC) within the cloud varies linearly with height. The latter two assumptions are in closer conformity with in-situ observations. Algorithms that can retrieve both the DVP and cloud liquid water path (LWP) are presented. The cloud LWPs derived based on the retrieved DVPs are more sound than those obtained from assuming a vertical-constant DER profile. To enhance the DVP retrievals, a split-window technique is presented to better estimate the amount of above-cloud precipitable water (PW). The retrieval algorithms are applied to the MODIS Level-1B 1-km data and presently tested for two stratiform cloud cases observed over the north-central Oklahoma where independent cloud microphysics data are available from the United States Department of Energy's Atmospheric Radiation Measurement (ARM) Program. Good agreements in the retrieved DER profile, LWP, and above-cloud PW are found in a preliminary demonstration of the new approach. Sensitivity of the retrieved DER profile to uncertainties in the above-cloud PW and surface albedos is also discussed. *INDEX TERMS*: 0320 Atmospheric Composition and Structure: Cloud physics and chemistry; 0394 Atmospheric Composition and Structure: Instruments and techniques; 3359 Meteorology and Atmospheric Dynamics: Radiative processes; 3360 Meteorology and Atmospheric Dynamics: Remote sensing; *KEYWORDS*: MODIS, droplet effective radius, cloud microphysics profile

**Citation:** Chang, F.-L., and Z. Li, Retrieving vertical profiles of water-cloud droplet effective radius: Algorithm modification and preliminary application, *J. Geophys. Res.*, 108(D24), 4763, doi:10.1029/2003JD003906, 2003.

### 1. Introduction

[2] Planetary boundary layer clouds have the most significant influence on cloud radiative forcing due to their areal extent and frequent occurrence [*Harrison et al.*, 1990; *Hartmann et al.*, 1992]. Radiation absorbed by these clouds also plays an important role in cloud evolution and affects water redistribution [*Stephens*, 1999]. Since cloud morphological properties are an ensemble of cloud microphysics and cloud optical properties are governed by cloud microphysical properties, the most fundamental cloud variables are cloud microphysics that can influence the radiative transfer, droplet growth,

and precipitation processes in clouds [*International Panel on Climate Change (IPCC)*, 2001]. To fully understand these influences, we must have reliable information on the cloud microphysics, namely, droplet effective radius (DER) and liquid water path (LWP), which have been overlooked to some extent. Besides, we need to study if any changes in cloud LWP are related to variation in the DER. Derivation of cloud LWP from cloud optical depth and DER is vulnerable to errors in the retrieved DER [*Stephens*, 1978].

[3] Satellite observations provide the only means of acquiring global and long-term cloud DER measurements. Almost all previous satellite-based studies employed DER values retrieved from the NOAA Advanced Very High Resolution Radiometer (AVHRR) 3.7- $\mu\text{m}$  channel. A great deal of knowledge on cloud DER has been gained primarily by means of the AVHRR 3.7- $\mu\text{m}$  data. Investigations along this line were carried out for various purposes [e.g., *Kaufman and Nakajima*, 1993; *Han et*

<sup>1</sup>Also at Department of Meteorology, University of Maryland, College Park, Maryland, USA.

al., 1994, 1998; Platnick and Twomey, 1994; Nakajima and Nakajima, 1995; Rosenfeld and Lensky, 1998; Chang et al., 2000; Coakley et al., 2000; Szczodrak et al., 2001]. However, there are cons and pros in the retrievals of cloud DER using the 3.7- $\mu\text{m}$  channel because the radiance measurements at this wavelength are overly sensitive to droplet absorption occurring near the cloud top. There is a large uncertainty that the retrieved DER lacks representation for the entire cloud column [Platnick, 2000; Chang and Li, 2002].

[4] Relative to the AVHRR, the Moderate-resolution Imaging Spectroradiometer (MODIS) on board the Terra and Aqua platforms of the NASA Earth Observing System (EOS) offers numerous advances that can considerably improve the retrieval of cloud properties. They include, among many others, on-board calibrations and 36-channel high spectral and spatial resolutions [King et al., 1992, 2003]. There are three useful channels for cloud DER retrievals, namely, 1.6  $\mu\text{m}$ , 2.1  $\mu\text{m}$ , and 3.7  $\mu\text{m}$  [Platnick et al., 2003]. Because of the varying strengths of cloud droplet absorption at these different spectral bands, DER retrievals from the three channels represent different layers within the cloud, i.e., the 3.7- $\mu\text{m}$  retrieval corresponds to the DER at very top layer of the cloud, whereas the 2.1- $\mu\text{m}$  and 1.6- $\mu\text{m}$  retrievals correspond to the DER values somewhat deeper inside the cloud. Due to the gradual variation in the weighting function of radiance reflected from different layers, it is hard to assign the retrievals from the three channels to any particular cloud level [Platnick, 2000; Chang and Li, 2002]. In the previous study, Chang and Li [2002] showed a feasible approach by assumed that the DER has a linear vertical distribution with respect to the in-cloud optical depth. They attempted to retrieve the DER vertical profile (DVP) by utilizing simulated multispectral near-infrared (NIR) reflectances from *in-situ* cloud microphysics data and tested their retrieved DVP by comparing with the observed one.

[5] This paper exploits the utility of the MODIS Level-1B 1-km NIR measurements at 1.6  $\mu\text{m}$ , 2.1  $\mu\text{m}$  and 3.7  $\mu\text{m}$  for the retrieval of the DVP. Three approaches, including the method of Chang and Li [2002] and two modified methods that also assumed linear vertical variations of cloud DER and liquid water content (LWC), but with respect to geometry height within cloud, are explored and compared for their DVP retrievals. A preliminary validation is provided by comparing the MODIS satellite-retrieved DVP to the ground-based DVP retrieved from the cloud profiling radar measurements at the ARM Southern Great Plains (SGP) site in the north-central Oklahoma. Section 2 describes the three analytic DVPs. Section 3 presents the split-window method for determining the column precipitable water (PW) above the cloud. Such determination of the above-cloud PW is designed to more accurately account for the water vapor attenuation in the satellite radiance measurements. Section 4 presents the procedure for retrieving the DVPs and associated cloud properties with case analysis from the MODIS data. Section 5 presents the computation of the cloud LWP based on the MODIS-retrieved DVP and compares it with those computed by assuming a constant DER column. Comparisons with

the ARM ground-based DVP and LWP retrievals are also discussed. Section 6 gives the concluding remarks.

## 2. Three Analytic Droplet Effective Radius (DER) Vertical Profiles

[6] Cloud property retrievals are commonly based on the assumption that cloud DER is invariant with height. However, observational data as reviewed by Miles et al. [2000] have shown that cloud DER often varies monotonically between cloud top and cloud base. NIR reflectances at multispectral wavelengths such as 1.6  $\mu\text{m}$ , 2.1  $\mu\text{m}$  and 3.7  $\mu\text{m}$  can have different penetration path lengths into the cloud and convey certain information concerning the DVP. However, this information alone is insufficient to allow for the retrieval of any DER profile without a priori knowledge of the vertical weightings of the reflectance [Platnick, 2000]. To overcome this difficulty, Chang and Li [2002] assumed a linear DVP (hereafter referred to as DVP1) where the DER ( $r_e$ ) is linearly proportional to the in-cloud optical depth ( $\tau'$ ), where  $\tau' = \tau/\tau_c$  and  $\tau_c$  denotes the cloud optical depth.

[7] Since *in-situ* measurements have shown that cloud DER often increases with the geometrical height [compare Miles et al., 2000], the DVP is modified accordingly such that  $r_e \propto z'$  (hereafter referred to as DVP2), where  $z' = (z - z_{\text{top}})/(z_{\text{base}} - z_{\text{top}})$  denotes the fractional cloud height with  $z' = 0$  for cloud top and  $z' = 1$  for cloud base. A third DVP is also studied where the assumption is that the LWC changes linearly with height (referred to as DVP3), which is the case for clouds formed from adiabatic processes.

[8] In this study, the three analytic DVPs are adopted, namely, DVP1:  $dr_e/d\tau = \text{constant}$ , DVP2:  $dr_e/dz = \text{constant}$ , and DVP3:  $d\text{LWC}/dz = \text{constant}$ . The relationships between  $dr_e/d\tau$ ,  $dr_e/dz$ , and  $d\text{LWC}/dz$  are presented in the Appendix, which allow for conversion and comparison among the three DVPs. It is shown that  $dr_e/dz = \text{constant}$  (DVP2) is equivalent to  $dr_e^3/d\tau = \text{constant}$ ; and  $d\text{LWC}/dz = \text{constant}$  (DVP3) is equivalent to  $dr_e^3/dz = \text{constant}$  ( $\text{LWC} \propto r_e^3$ ) or  $dr_e^5/d\tau = \text{constant}$ . To compare their performance, the three DVP models can thus be expressed as functions of  $\tau'$  by, respectively,

$$\text{DVP1} : r_e(\tau') = r_{e1} + (r_{e2} - r_{e1})\tau', \quad (1)$$

$$\text{DVP2} : r_e(\tau') = [r_{e1}^3 + (r_{e2}^3 - r_{e1}^3)\tau']^{1/3}, \quad (2)$$

$$\text{DVP3} : r_e(\tau') = [r_{e1}^5 + (r_{e2}^5 - r_{e1}^5)\tau']^{1/5}, \quad (3)$$

where  $r_{e1}$  denotes the DER at the cloud top (i.e.,  $\tau' = \tau = 0$ ) and  $r_{e2}$  denotes the DER at the cloud base (i.e.,  $\tau' = 1$  and  $\tau = \tau_c$ ).

[9] Figure 1 illustrates the different vertical structures of the three DVPs for a decreasing DER (a) from the cloud top ( $r_{e1} = 12 \mu\text{m}$ ) to cloud base ( $r_{e2} = 6 \mu\text{m}$ ) and for an increasing DER (b) from the cloud top ( $r_{e1} = 6 \mu\text{m}$ ) to cloud base ( $r_{e2} = 12 \mu\text{m}$ ). For retrieving the DER, the 3.7- $\mu\text{m}$  reflectance depends largely on the very top layer of

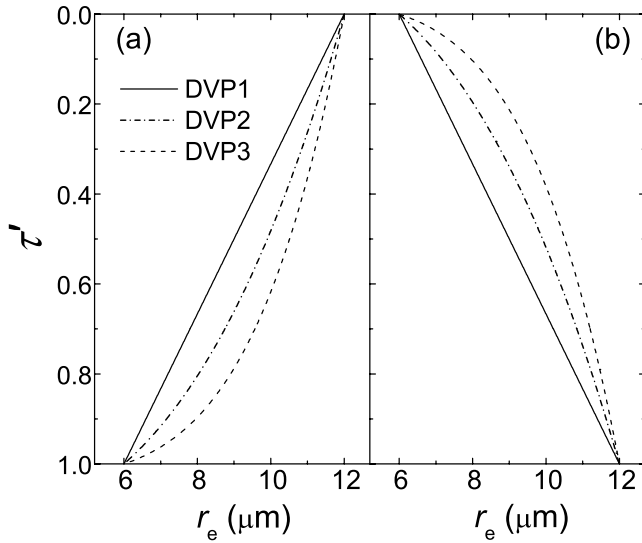


**Figure 1.** Schematic plot for the three analytic DVPs as described in the text. (a)  $r_{e1} = 12 \mu\text{m}$  and  $r_{e2} = 6 \mu\text{m}$ ; (b)  $r_{e1} = 6 \mu\text{m}$  and  $r_{e2} = 12 \mu\text{m}$ .

the cloud so is mainly affected by  $r_{e1}$ ; whereas the shorter wavelengths like the 2.1- $\mu\text{m}$  and 1.6- $\mu\text{m}$  reflectances have more bearing on the deeper cloud and are thus more affected by  $r_{e2}$ . The different dependencies of the three NIR reflectances

on  $r_{e1}$  and  $r_{e2}$  lay the foundation for the retrieval of an optimal DVP [Chang and Li, 2002].

### 3. Determination of the Above-Cloud Precipitable Water

[10] In retrieving the DER, knowing the amount of above-cloud PW is necessary in order to account for the water vapor attenuation in the satellite radiance measurements. Conventionally, the above-cloud PW is often determined from reanalysis data such as those from the National Centers for Environmental Prediction (NCEP), or by using estimates from some standard atmospheric model. Here, a split-window technique is presented for the determination of the above-cloud PW. The retrieval principle is based on the different absorption strengths of water vapor at the 11- $\mu\text{m}$  and 12- $\mu\text{m}$  channels, where the brightness temperature difference between the two channels ( $\text{BTD} = T_{11} - T_{12}$ ) has a large dependence on the above-cloud PW. This technique has been previously used to determine the total PW for clear sky conditions [e.g., Chesters et al., 1983; Kleespies and McMillin, 1984].

[11] Figure 2 shows the BTD as a function of the above-cloud PW for various conditions of satellite viewing zenith angle ( $\theta$ ), cloud optical depth ( $\tau_c$ , defined at the 0.64- $\mu\text{m}$  wavelength), DER, cloud top temperature ( $T_c$ ), and ground surface temperature ( $T_g$ ). These results are obtained using

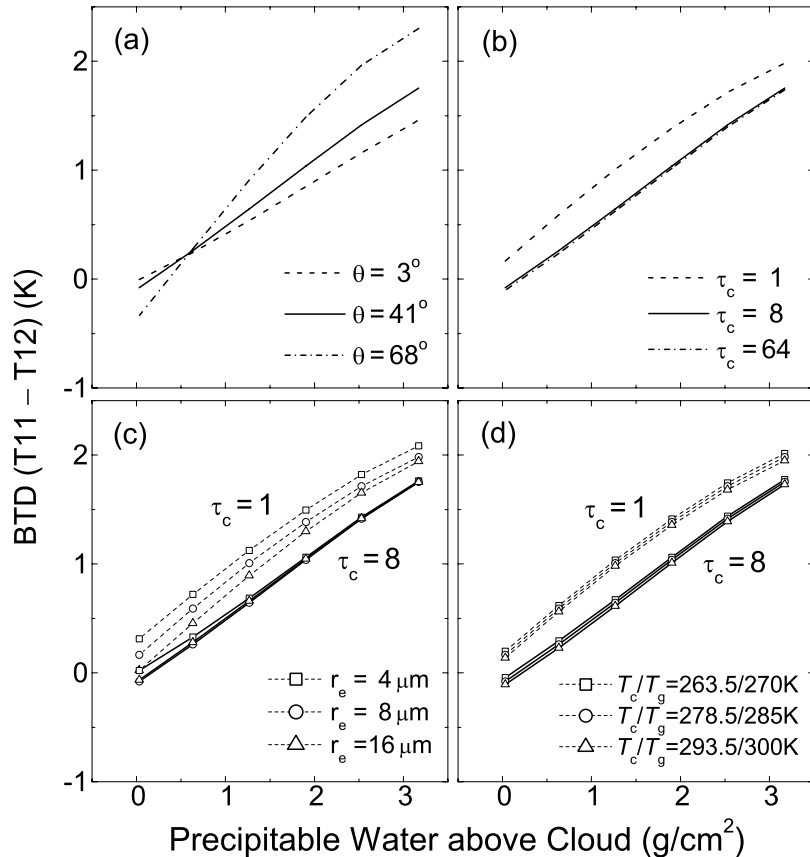


**Figure 2.** Model-simulated brightness-temperature difference ( $\text{BTD} = T_{11} - T_{12}$ ) versus the above-cloud PW for (a) three  $\theta$  ( $\tau_c = 8$ ,  $r_e = 8 \mu\text{m}$  and  $T_c/T_g = 278.5/285\text{K}$ ); (b) three  $\tau_c$  ( $\theta = 41.1^\circ$ ,  $r_e = 8 \mu\text{m}$  and  $T_c/T_g = 278.5/285\text{K}$ ); (c) three  $r_e$  with  $\tau_c = 1$  and 8 ( $\theta = 41.1^\circ$  and  $T_c/T_g = 278.5/285\text{K}$ ); and (d) three  $T_c/T_g$  with  $\tau_c = 1$  and 8 ( $\theta = 41.1^\circ$  and  $r_e = 8 \mu\text{m}$ ).

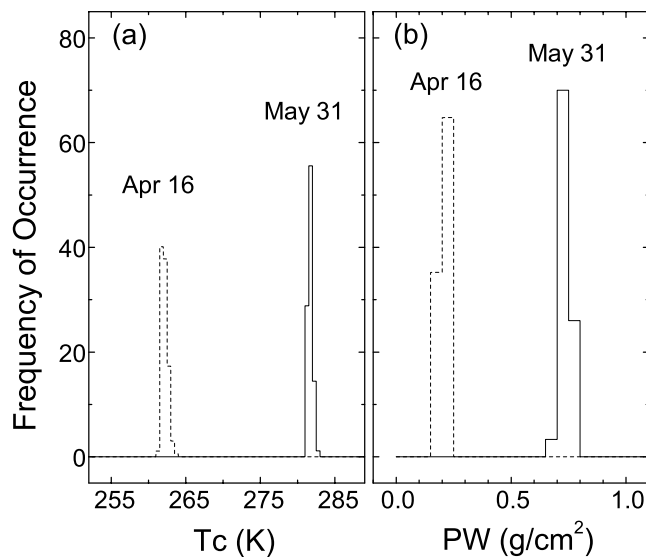


**Figure 3.** Frequency distributions of the pixel-scale  $T_c$  (a) and the above-cloud PW (b) observed on April 16 and May 31, 2001 from a  $(10 \text{ km})^2$  area centered at the ARM SGP site.

the adding-doubling radiative transfer model with a water cloud layer placed between 0.5–1.0 km. The atmospheric transmissions are calculated using MODTRAN-4 [Berk *et al.*, 1999]. Various atmospheric temperature profiles based on  $T_g$  and a fixed lapse rate of  $\Gamma = 6.5 \text{ K/km}$  were used in calculating the thermal emission. Temperature of the tropopause was set to 216 K and the U.S. standard atmospheric temperature profile was used for above the tropopause. The figure shows a positive relationship between the BTD and above-cloud PW, which depends largely on  $\theta$  (Figure 2a). Some dependencies are also shown on  $\tau_c$  (Figure 2b),  $r_e$  (Figure 2c), and the temperatures of cloud top ( $T_c$ ), atmosphere, and surface ( $T_g$ ) (Figure 2d), but these dependences diminish as  $\tau_c$  increases; for example, when  $\tau_c = 8$ , the dependences are less significant (cf. Figures 2b–2d). Note that in Figure 2d the atmospheric temperature profile was modeled with a fixed lapse rate of  $\Gamma = 6.5 \text{ K/km}$ , thus  $T_c = T_g - 6.5 \text{ K}$  for a cloud-top height at 1 km.

[12] The retrieval method was applied to the Terra/MODIS Level-1B 1-km data gathered at the ARM SGP site for two stratiform cloud cases observed on April 16 (1725 UTC) and May 31 (1655 UTC), 2001. Figure 3 shows the frequency distributions of (a) cloud-top temperature ( $T_c$ ) and (b) above-cloud PW retrieved from a  $(10 \text{ km})^2$  area centered at the SGP site on the two days. The ARM ground-based measurements of cloud-top/cloud-base heights and temperatures, and the above-cloud PW are given in Table 1. The MODIS satellite-based retrievals of  $T_c$  are quite uniform with a mean  $T_c = 262.4 \text{ K}$  on April 16 and  $281.9 \text{ K}$  on May 31, which are in good agreement with the ground-based measurements.

[13] The satellite-retrieved cloud-top height ( $z_{\text{top}}$ ) is estimated based on  $z_{\text{top}} = z_g + (T_g - T_c)/\Gamma$ , where  $T_g$  is 289.6 K on April 16 and 290.6 K on May 31. Since  $z_g \approx 0.3 \text{ km}$  for the SGP site, the mean  $z_{\text{top}}$  are estimated to be 4.5 km and 1.6 km respectively on the two days, which are close to the radiosonde measurements of 4.8 km on April 16 and 1.5 km

on May 31. Note that the cloud-base heights are roughly 3.3 km and 0.8 km, respectively, as indicated by the ARM SGP balloon-borne radiosonde data acquired at 1731 UTC on April 16 and at 1736 UTC on May 31 at Lamont, Oklahoma ( $36.61^\circ \text{N}$ ,  $97.49^\circ \text{W}$ ). As for the above-cloud PW, the satellite retrievals have a mean value of about  $0.20 \text{ g/cm}^2$  on April 16 and  $0.77 \text{ g/cm}^2$  on May 31; both agreed well with the ARM measurements, especially the MWR-based estimates. It is widely known that the magnitude of MWR-based PW estimates is more reliable than the radiosonde data [e.g., Guichard *et al.*, 2000; Turner *et al.*, 2003].

## 4. Procedure for Retrieving DER Vertical Profile (DVP)

### 4.1. Retrieval Procedure

[14] In retrieving the DVP, an iterative retrieval scheme similar to the conventional DER retrieval scheme is employed, except that a variant vertical profile denoted by  $r_{e1}$  and  $r_{e2}$  is retrieved, instead of a constant  $r_e$ . The iterative procedure starts by retrieving  $\tau_c$  from the visible ( $0.64\text{-}\mu\text{m}$ ) channel, and is followed by retrieving  $r_{e1}$  and  $r_{e2}$  from the three NIR channels, above-cloud PW from the split-window channels, and  $T_c$  from the  $11\text{-}\mu\text{m}$  channel. The retrieval procedure is repeated until an acceptable level of convergence is achieved. It is to note that in retrieving  $r_{e1}$  and  $r_{e2}$ , this study uses a bi-spectral NIR retrieval algorithm [Chang *et al.*, 2002], rather than applying the least squares statistical approach to all three NIR channels simultaneously as described in Chang and Li [2002]. This is mainly due to the difficulty of the least squares approach that requires massive lookup tables from radiative transfer calculations for more than six dimensions (i.e.,  $\tau$ ,  $r_{e1}$ ,  $r_{e2}$ ,  $z_{\text{top}}$ , and three angles, including solar and viewing zeniths and their relative azimuth). The bi-spectral retrieval approach can significantly reduce the demand for computer memory and computing time, which is essential for processing a large volume of the MODIS data.

[15] The bi-spectral retrieval procedure is applied to two separate combinations of 1)  $3.7\text{-}\mu\text{m}$  plus  $1.6\text{-}\mu\text{m}$  channels and 2)  $3.7\text{-}\mu\text{m}$  plus  $2.1\text{-}\mu\text{m}$  channels to retrieve two separate sets of DVP. Final DVP retrieval is determined as the mean of the two DVPs. The bi-spectral retrieval procedure begins with retrieving two separate DERs from two individual NIR channels, for instance,  $r_{e-3.7}$  from the  $3.7\text{-}\mu\text{m}$  channel and  $r_{e-1.6}$  from the  $1.6\text{-}\mu\text{m}$  channel. This step is similar to the conventional method that assumes a vertically invariant DER profile. However, if the cloud layer has a variant DER profile, the retrieved  $r_{e-1.6}$  will differ from  $r_{e-3.7}$  because photon transports deeper inside cloud at  $1.6 \mu\text{m}$  than at

**Table 1.** Ground-Based Measurements of Cloud-Top/Cloud-Base Heights and Temperatures, Cloud Optical Depth and the Above-Cloud PW

	April 16	May 31
Cloud-top height (km)	4.8	1.5
Cloud-base height (km)	3.3	0.8
Cloud-top temperature (K)	261.4	283.1
Cloud-base temperature (K)	269.3	285.7
Cloud optical depth	66.5	37.4
Radiosonde PW ( $\text{g/cm}^2$ )	0.14	1.15
MWR PW ( $\text{g/cm}^2$ )	0.16	0.87

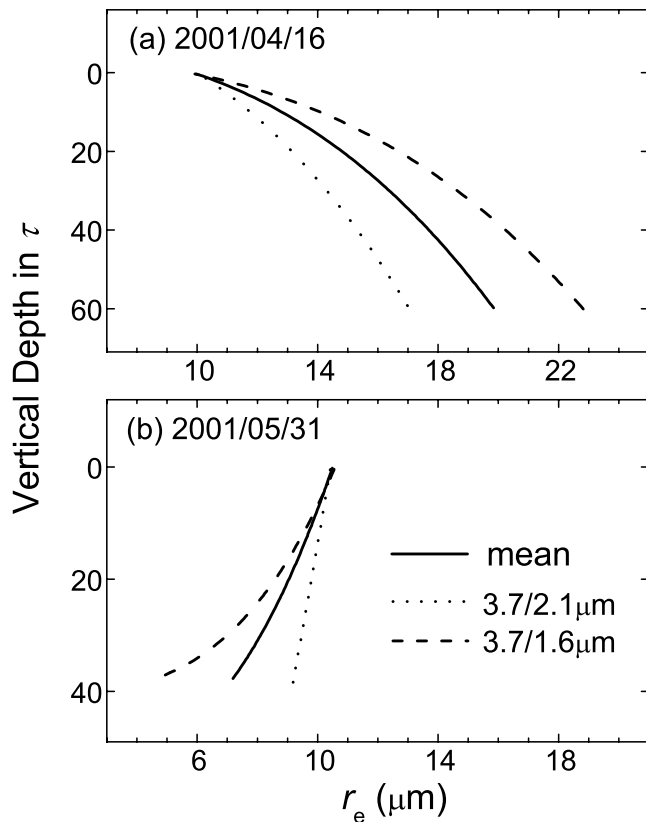


**Figure 4.** Comparisons of mean DVP retrieved using all three NIR channels (solid curves) with those using the 3.7- $\mu\text{m}$ /2.1- $\mu\text{m}$  channels (dotted curves) and the 3.7- $\mu\text{m}$ /1.6- $\mu\text{m}$  channels (dashed curves) versus the vertical depth in  $\tau$ . The retrievals are obtained using the DVP2 model for two stratiform clouds observed on April 16 (a) and May 31 (b), 2001 from a  $(10 \text{ km})^2$  area centered at the ARM SGP site.

3.7  $\mu\text{m}$ . The difference ( $\Delta r_e$ ) between the retrieved values of  $r_{e-3.7}$  and  $r_{e-1.6}$  can then be used to infer a DVP. The next step is to repeat the retrievals at 3.7  $\mu\text{m}$  and at 1.6  $\mu\text{m}$ , but using lookup tables that were generated based on various DVPs constrained by  $r_{e1}$  for the cloud top and  $r_{e2} = r_{e1} + \Delta r_e$  for the cloud base. This retrieval step is repeated by increasing  $\Delta r_e$  until the two newly retrieved values of  $r_{e-3.7}$  and  $r_{e-1.6}$  converge, which usually requires three to four times to reach convergence.

#### 4.2. Case Analysis

[16] Figure 4 shows the mean DER profiles (solid curves) retrieved using the DVP2 model from the MODIS Level-1B 1-km data for two stratiform clouds observed on April 16 (a) and May 31 (b), 2001. The mean DER profile is obtained for a  $(10 \text{ km})^2$  area (i.e.,  $10 \times 10$  pixels) centered at the ARM SGP site in north central Oklahoma and is plotted against the in-cloud optical depth ( $\tau$ ). The retrieved  $r_{e1}$ ,  $r_{e2}$  and  $\tau_c$  are  $9.9 (\pm 0.5) \mu\text{m}$ ,  $19.8 (\pm 2.4) \mu\text{m}$ , and  $61.3 (\pm 9.5)$  for Figure 4a and  $10.5 (\pm 1.0) \mu\text{m}$ ,  $7.2 (\pm 2.0) \mu\text{m}$ , and  $38.7 (\pm 4.2)$  for Figure 4b, respectively. The mean DVPs retrieved using only two NIR channels, i.e., 3.7- $\mu\text{m}$ /2.1- $\mu\text{m}$  (dotted curves) and 3.7- $\mu\text{m}$ /1.6- $\mu\text{m}$  (dashed curves), are also plotted in each sub-panel. It is seen that the retrieved DVPs

exhibit more vertical variation with the 3.7- $\mu\text{m}$ /1.6- $\mu\text{m}$  channels than with the 3.7- $\mu\text{m}$ /2.1- $\mu\text{m}$  channels. This can be attributed to that the 1.6- $\mu\text{m}$  channel has a larger photon penetration depth than the 2.1- $\mu\text{m}$  channel and therefore the former captures more the DER deeper inside the cloud.

[17] Figure 5 compares the three mean DVPs retrieved based on DVP1, DVP2, and DVP3 (three black curves) for the two stratiform clouds shown in Figure 4. Each sub-panel represents for a  $(5 \text{ km})^2$  area (i.e.,  $5 \times 5$  pixels), where mean latitude and longitude are indicated. Two light-gray curves indicate the mean  $\pm$  one standard deviation of the  $5 \times 5$  pixels (only shown for the DVP2 retrievals, but similar in magnitude for DVP1 and DVP3). Generally speaking, the three DVP retrievals are similar in trend, with an increasing DER from cloud top to cloud base (Figure 5a) and a decreasing DER from cloud top to cloud base (Figure 5b). They are nearly the same in the upper portion of the profiles, but deviate further toward cloud base. This is understandable as the NIR reflectances are mostly affected by the DER near the cloud top. The larger discrepancies toward cloud base are consistent with the error analysis given in Chang and Li [2002], which showed that the retrieved DER near cloud base is subject to larger uncertainty than near cloud top.

[18] The different behaviors of the DER profile on the two days may be related to different cloud development stages. The case of May 31 has a typical vertical profile of DER that increases from cloud base to cloud top, whereas the case of April 16 has an inverted DER profile that increases toward cloud base. Although there was no precipitation observed from below the clouds at the MODIS passing time, the increasing DER on April 16 may be affected by light drizzle occurred near cloud base, where the ground-based radar reflectivity measurements rose above  $-20 \text{ dBZ}$ . Frisch et al. [1995] have demonstrated that at such radar reflectivity factors light drizzle was frequently found. Another cause for the larger DER can be the presence of ice-phased particles. Ice has a much larger absorbing efficiency than water, especially at the 1.6- $\mu\text{m}$  channel [e.g., Pilewskie and Twomey, 1987]. The cloud temperatures on this date ranged about 261 K–269 K. If ice were present, the small ice crystals can appear as a water cloud containing larger droplets, but it can not be verified.

[19] Since the DVP2 falls in the middle of the three, it is recommended to use this profile if no other information indicates otherwise. Besides, the assumption that the DER varies proportional to the geometrical height in DVP2 is in closer conformity with *in-situ* observations than the assumption that the DER varies proportional to in-cloud optical depth in DVP1. Of course, if a cloud system is known to follow an adiabatic process, DVP3 shall be considered. Comparisons on the retrieved DER profile and LWP with ground-based retrievals are therefore focused on the DVP2 model in the following section.

#### 4.3. Retrieval Sensitivity

[20] The retrieval lookup tables were generated using an adding-doubling radiative transfer model [Chang and Li, 2002]. A Lambertian surface albedo of 0.2 was used for the three NIR channels and a value of 0.05 was used for the visible channel. The DVP retrievals are tested for its sensitivity to (1) the above-cloud PW for the changes of

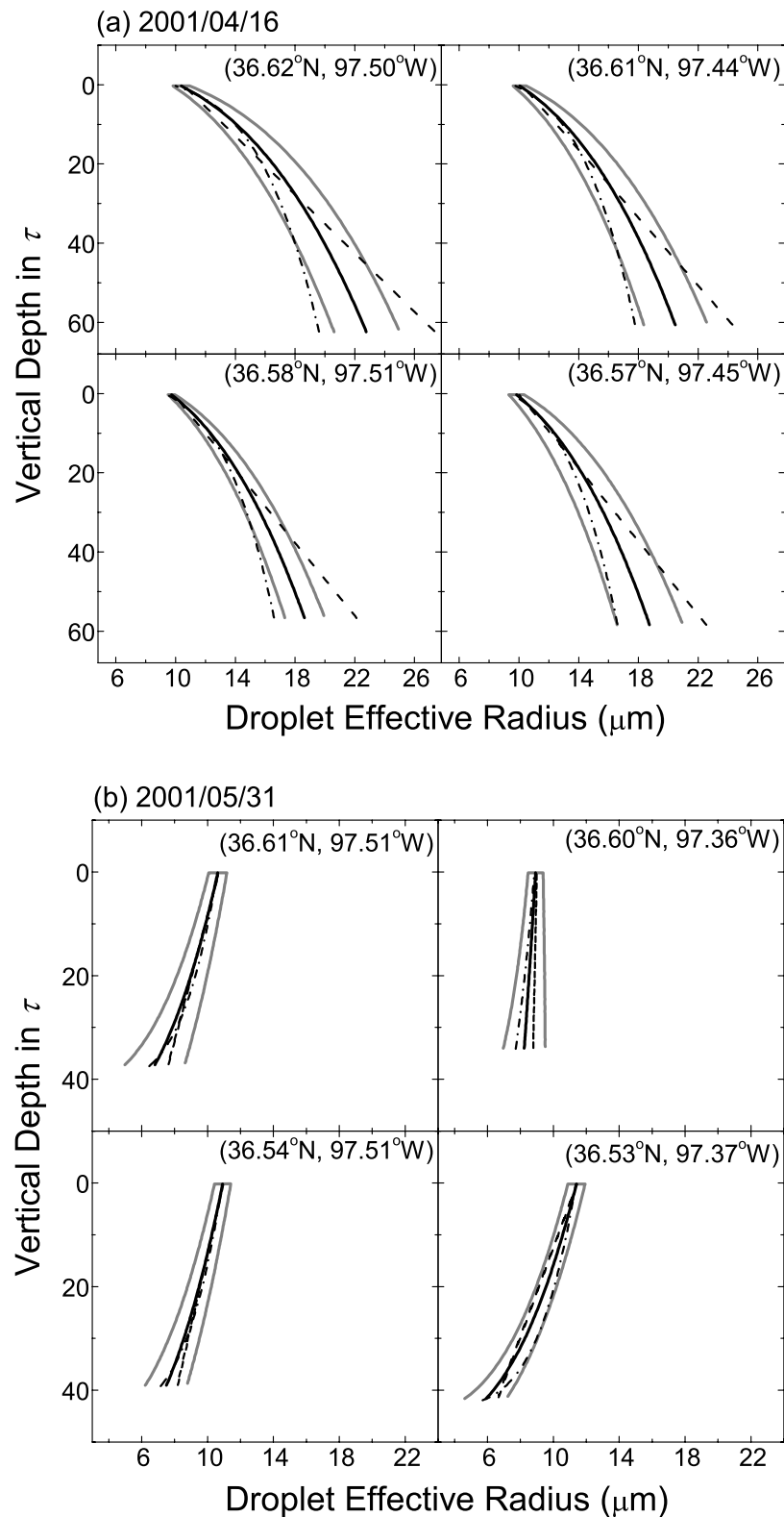


**Figure 5.** Comparisons of DVPs retrieved using DVP1 (dashed), DVP2 (solid), and DVP3 (dash-dot) for two stratiform clouds observed on April 16 (a) and May 31 (b), 2001 as shown in Figure 4. Each sub-panel showed retrievals obtained from a  $(5 \text{ km})^2$  area, so a total area of  $(10 \text{ km})^2$ . Light gray curves indicate the mean  $\pm$  one standard deviation for the uncertainty of the DVP2 retrievals. The uncertainty is similar in magnitude for DVP1 and DVP3 (not shown). Mean solar zenith, viewing zenith, and relative azimuth angles are  $(29.7^\circ, 10.2^\circ, 132^\circ)$  for (a) and  $(24.4^\circ, 53.2^\circ, 155^\circ)$  for (b).

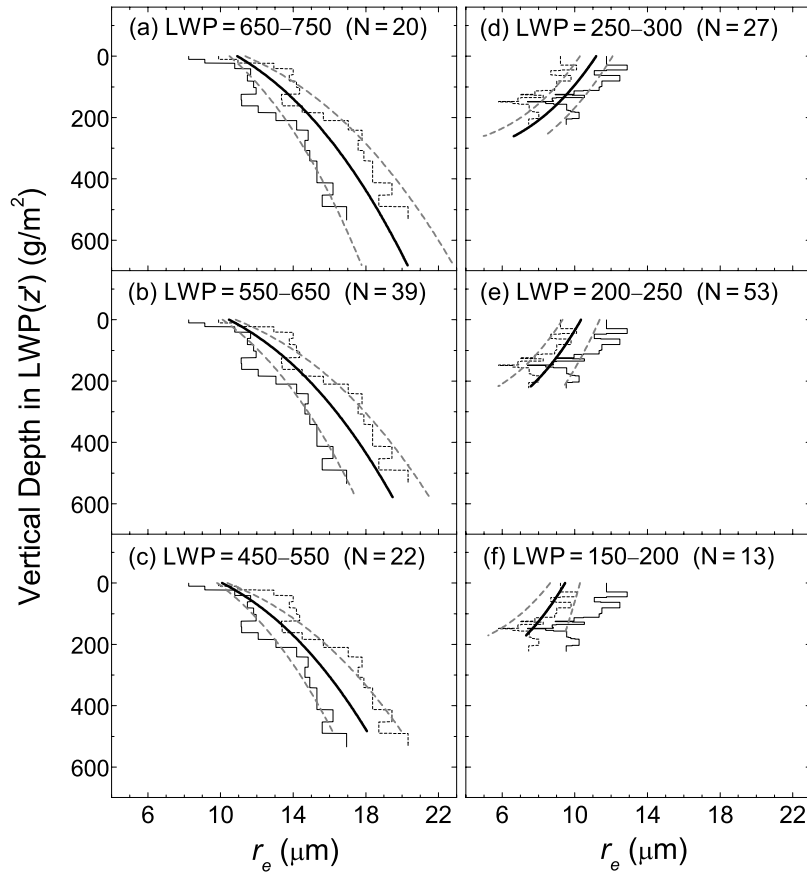


**Figure 6.** Comparisons of MODIS-DVP2 (smooth curves) and ground (jagged) retrieved DER profiles against the vertical depth in  $LWP(z')$  ( $\text{g/m}^2$ ) for two stratiform clouds observed on April 16 (a–c) and May 31 (d–f), 2001 as shown in Figure 5. Three sub-panels on each day show different ranges of cloud LWP and  $N$  denotes the number of MODIS pixels sampled in the indicated cloud LWP range. The MODIS DVPs are shown in mean (solid)  $\pm$  one standard deviation (dashed). The ground-retrieved DVPs are derived using two retrieval schemes of Dong and Mace (solid jagged) and Frisch et al. (dotted jagged) as both are plotted identically in the three sub-panels for each day.

$\pm 0.3 \text{ g/cm}^2$  and (2) surface albedos for the changes of  $\pm 0.2$  in all three NIR channels and a change of  $+0.1$  in the visible channel. The resulted changes in  $r_{e1}$  and  $r_{e2}$  are shown in Table 4 for the combinations of  $3.7\text{-}\mu\text{m}/2.1\text{-}\mu\text{m}$  and  $3.7\text{-}\mu\text{m}/1.6\text{-}\mu\text{m}$  using the DVP2 model. In general, the above-cloud PW has more influence on the retrievals of both  $r_{e1}$  and  $r_{e2}$  than the surface albedo. This is because of thick clouds occurred on the two days. Table 4 also compares the sensitivity for an assumed case of  $\tau_c = 10$ , which shows slight increases of the retrieval sensitivity to changes in surface albedos. Overall, the effects of above-cloud PW and surface albedos on the DVP retrievals are small for moderate to optically thick clouds.

[21] Note that the focus of this paper is on modifications to a previously reported methodology and on demonstration of the performance of these modifications in retrieving the DER profiles. The strengths and weaknesses of the method are currently examined for stratiform clouds. The applicability to convective clouds remains to be tested. More comprehensive validation study is in progress, which will thoroughly evaluate various cloud conditions that favor or disfavor the application of the method presented in this

study [F.-L. Chang, Z. Li, and X. Dong, A comparison of cloud vertical profiles of droplet effective radius and liquid water path as deduced from the MODIS satellite and ARM ground measurements, manuscript in preparation, 2003].

## 5. Computation of Liquid Water Path

[22] Cloud LWP is defined by

$$LWP = \int_{z_{\text{top}}}^{z_{\text{base}}} LWC(z) dz, \quad (4)$$

where  $z_{\text{top}}$  and  $z_{\text{base}}$  denote the cloud-top and cloud-base heights, respectively. The relationship between cloud optical depth  $\tau_c$ , LWC, and  $r_e$  is given (see Appendix) by

$$\tau_c = \frac{3Q_{\text{ext}}}{4\rho_w} \int_{z_{\text{top}}}^{z_{\text{base}}} \frac{LWC(z)}{r_e(z)} dz, \quad (5)$$

where  $Q_{\text{ext}}$  is the extinction efficiency ( $\approx 2$ ) and  $\rho_w$  is the density of water. In conventional remote sensing applica-

**Table 2.** Retrievals of Mean DER Profile (viz.  $r_{e1}$  and  $r_{e2}$  in  $\mu\text{m}$ ) and  $\tau_c$  From Three Analytic DVP1, DVP2 and DVP3 and Retrievals of Mean  $r_e$  ( $\mu\text{m}$ ) From Three Single NIR Channels at 3.7  $\mu\text{m}$ , 2.1  $\mu\text{m}$  and 1.6  $\mu\text{m}$ , Respectively<sup>a</sup>

	April 16			May 31		
	Figure 5a	Figure 5b	Figure 5c	Figure 5d	Figure 5e	Figure 5f
DVP1: $r_{e1}$	10.4 (0.3)	10.1 (0.3)	9.8 (0.3)	11.2 (0.9)	10.4 (1.0)	9.5 (0.8)
$r_{e2}$	25.0 (2.9)	23.0 (3.1)	21.9 (2.7)	7.8 (2.1)	7.8 (1.9)	7.7 (1.8)
$\tau_c$	64.7 (7.1)	58.2 (6.5)	52.4 (4.7)	42.8 (3.1)	37.8 (2.8)	31.8 (2.9)
DVP2: $r_{e1}$	10.3 (0.2)	9.8 (0.4)	9.6 (0.4)	11.1 (0.9)	10.3 (1.0)	9.5 (0.8)
$r_{e2}$	20.3 (2.5)	19.5 (2.0)	18.1 (1.9)	6.6 (1.7)	7.6 (1.8)	7.3 (2.1)
$\tau_c$	66.2 (7.6)	57.5 (6.1)	52.6 (5.1)	43.4 (2.6)	37.6 (2.5)	31.9 (2.9)
DVP3: $r_{e1}$	10.0 (0.3)	9.6 (0.4)	9.3 (0.3)	11.2 (0.5)	10.3 (1.1)	9.4 (0.8)
$r_{e2}$	17.9 (1.6)	17.1 (1.7)	16.4 (1.3)	6.5 (1.0)	7.5 (1.7)	7.0 (1.8)
$\tau_c$	65.9 (6.2)	57.4 (5.7)	51.9 (4.5)	43.9 (2.3)	37.7 (2.5)	32.0 (3.0)
3.7- $\mu\text{m}$ $r_e$	10.7 (0.3)	10.3 (0.3)	10.0 (0.3)	11.1 (0.8)	10.3 (0.9)	9.4 (0.8)
2.1- $\mu\text{m}$ $r_e$	11.4 (0.4)	10.8 (0.4)	10.5 (0.3)	10.9 (0.6)	10.2 (0.8)	9.4 (0.8)
1.6- $\mu\text{m}$ $r_e$	12.9 (0.7)	12.8 (0.7)	12.7 (0.7)	9.9 (0.6)	9.3 (0.7)	8.7 (0.6)

<sup>a</sup>Results are obtained for the data corresponding to Figure 5 (plotted for DVP2 only). In the parentheses is the standard deviation associated with the mean.

tions,  $r_e$  is assumed to be independent of height, so cloud LWP is computed by

$$\text{LWP} = \frac{2}{3} \tau_c r_e. \quad (6)$$

The resulting cloud LWP is a biased value pending on the DER profile.

[23] To calculate cloud LWP using the retrieved DER profile, the three analytic DVPs given by Equations (1)–(3) in Section 2 can be rewritten in terms of  $z'$  through the relationship  $d\tau \sim r_e^2 dz$  (see Appendix) by

$$\text{DVP1} : r_e(z') = [r_{e1}^{-1} + (r_{e2}^{-1} - r_{e1}^{-1})z']^{-1}, \quad (7)$$

$$\text{DVP2} : r_e(z') = r_{e1} + (r_{e2} - r_{e1})z', \quad (8)$$

$$\text{DVP3} : r_e(z') = [r_{e1}^3 + (r_{e2}^3 - r_{e1}^3)z']^{1/3}, \quad (9)$$

where  $z' = (z - z_{\text{top}})/(z_{\text{base}} - z_{\text{top}})$  denotes the fractional height within cloud. Thus, the cloud LWP can be calculated for each pixel with the retrieved  $r_{e1}$ ,  $r_{e2}$  and  $\tau_c$  using equation (5). Since  $\text{LWC}(z')$  is proportional to  $r_e^3(z')$  (see Appendix A5), in fact, a vertical profile of  $\text{LWP}(z')$  as defined by integrating  $\text{LWC}(z')$  from the cloud top to a certain level  $z'$  can be calculated by

$$\text{LWP}(z') = \int_0^{z'} \text{LWC}(z) dz = \int_0^{z'} c_0 r_e^3(z) dz, \quad (10)$$

where  $c_0$  is a constant. Here, the integral of  $\text{LWP}(z')$  can be used to facilitate the comparisons with the vertical profile of LWC retrieved from the ground-based microwave radiometer (MWR) [Liljegren *et al.*, 2001] and the comparisons of DVPs in relation to  $\text{LWP}(z')$ .

[24] Figure 6 shows the retrieved DER profiles against the vertical depth in  $\text{LWP}(z')$  for the DVP2 retrievals obtained from the (10 km)<sup>2</sup> areas shown in Figures 4 and 5. Three sub-panels for three different ranges of total cloud LWP are shown in the left column (a–c) for April

16 and right column (d–f) for May 31. Plotted in each sub-panel are the DVP2 retrieval mean (dark solid curve) and the mean  $\pm$  one standard deviation (dark dashed curves), together with two ground-based DVP retrievals (gray jagged curves). The two ground-retrieved DVPs are derived using two different methods of Frisch *et al.* [1995] and Dong and Mace [2003], both are plotted identically in each of the three sub-panels for comparisons. The two ground-retrieved DVPs show similar trends because the two methods are applied to the same reflectivity data measured by ground-based cloud profiling radar, but different in magnitude because their parameterization schemes are different. It is seen that the MODIS-based and ground-based DVP retrievals agree well with differences less than 2  $\mu\text{m}$ , which is similar to the differences between the two ground-based radar retrievals. More importantly, all retrievals show similar trends in terms of their vertical variations.

[25] Tables 2 and 3 provide more details for the retrieval comparisons shown in Figure 6. Table 2 lists the means and the standard deviations for the retrieved  $r_{e1}$ ,  $r_{e2}$ , and  $\tau_c$  that were obtained by employing DVP1, DVP2, and DVP3, respectively. Table 2 also compares the conventional  $r_e$  that were retrieved using a single NIR channel from each of the 3.7- $\mu\text{m}$ , 2.1- $\mu\text{m}$ , and 1.6- $\mu\text{m}$  channels (bottom three rows). Noted that the DER retrieved using a single NIR channel is generally closer to the value of  $r_{e1}$  which is more representative of the cloud top. As a result, in computing cloud LWP using the single NIR retrieved DER (especially the 3.7- $\mu\text{m}$ ) would underestimate the LWP for an increasing DER profile

**Table 3.** Mean Cloud LWP ( $\text{g/m}^2$ ) Derived Based on the Three Retrieved DVP1, DVP2 and DVP3 and the Three  $r_e$  at 3.7  $\mu\text{m}$ , 2.1  $\mu\text{m}$  and 1.6  $\mu\text{m}$  as Shown in Table 2

	April 16			May 31		
	Figure 5a	Figure 5b	Figure 5c	Figure 5d	Figure 5e	Figure 5f
DVP1	799	664	573	267	224	176
DVP2	716	599	510	269	225	177
DVP3	655	547	473	278	227	177
3.7- $\mu\text{m}$	471	395	350	321	259	200
2.1- $\mu\text{m}$	502	414	368	315	256	200
1.6- $\mu\text{m}$	567	491	444	286	234	185

**Table 4.** Changes in the Retrieved  $r_{e1}$  ( $\mu\text{m}$ ) and  $r_{e2}$  ( $\mu\text{m}$ ) With Respect to Changes in Above-Cloud PW and Surface Albedos at NIR ( $\alpha_{\text{NIR}}$ ) and Visible ( $\alpha_{\text{VIS}}$ ) Wavelengths

$\Delta r_{e1}/\Delta r_{e2}$	April 16	May 31	$\tau_c = 10$
<b>PW + 0.3 g/cm<sup>2</sup>:</b>			
3.7- $\mu\text{m}$ /2.1- $\mu\text{m}$	-0.3/+0.9	-0.4/+1.2	-0.5/-0.5
3.7- $\mu\text{m}$ /1.6- $\mu\text{m}$	-0.3/+0.6	-0.4/+1.1	-0.3/-0.2
<b>PW - 0.3 g/cm<sup>2</sup>:</b>			
3.7- $\mu\text{m}$ /2.1- $\mu\text{m}$	+0.3/-1.4	+0.5/-1.4	+0.4/+0.4
3.7- $\mu\text{m}$ /1.6- $\mu\text{m}$	+0.2/-0.9	+0.5/-0.7	+0.2/+0.1
<b><math>\alpha_{\text{NIR}} + 0.2</math>:</b>			
3.7- $\mu\text{m}$ /2.1- $\mu\text{m}$	0.0/0.0	-0.0/+0.0	-0.1/+0.3
3.7- $\mu\text{m}$ /1.6- $\mu\text{m}$	0.0/0.0	-0.0/+0.4	+0.1/+1.5
<b><math>\alpha_{\text{NIR}} - 0.2</math>:</b>			
3.7- $\mu\text{m}$ /2.1- $\mu\text{m}$	0.0/0.0	+0.0/-0.0	+0.1/-0.3
3.7- $\mu\text{m}$ /1.6- $\mu\text{m}$	0.0/0.0	+0.0/-0.3	+0.1/-1.7
<b><math>\alpha_{\text{VIS}} + 0.1</math>:</b>			
3.7- $\mu\text{m}$ /2.1- $\mu\text{m}$	+0.0/+0.2	0.0/-0.1	0.0/-0.3
3.7- $\mu\text{m}$ /1.6- $\mu\text{m}$	-0.0/-0.2	0.0/-0.1	0.0/-1.1

from cloud top to cloud base; likewise it would overestimate the LWP for a decreasing DER profile from cloud top to cloud base. The over- or underestimation of the LWP depends on the strength of the droplet absorption, which is greatest at the 3.7- $\mu\text{m}$  channel.

[26] Table 3 compares the mean cloud LWPs derived from the retrievals presented in Table 2. The overall mean values ( $\text{g/m}^2$ ) are 673 (DVP1), 603 (DVP2), 553 (DVP3), 401 (3.7- $\mu\text{m}$ ), 423 (2.1- $\mu\text{m}$ ), and 496 (1.6- $\mu\text{m}$ ) for April 16; and 229 (DVP1), 231 (DVP2), 234 (DVP3), 268 (3.7- $\mu\text{m}$ ), 265 (2.1- $\mu\text{m}$ ), and 242 (1.6- $\mu\text{m}$ ) for May 31, respectively. The mean cloud LWP derived from the ground-based MWR measurements at the ARM SGP site for an average within  $\pm 10$  min of the MODIS passing time is  $535 \text{ g/m}^2$  on April 16 and is  $221 \text{ g/m}^2$  on May 31. Since satellite measurements are a snapshot over a large spatial domain whereas ground-based observations provide only point measurements in a time series, the differences between satellite-based and ground-based retrievals can be caused by the spatial and temporal variability. Nevertheless, the comparisons show that on April 16 cloud LWP derived based on DVP3 (i.e.,  $\text{LWC} \propto z$ ) has a better agreement with the ground-based retrieval; whereas on May 31 similar LWPs are derived from all three DVPs and agree well with the ground-retrieved value. In contrast, the LWPs computed based on a single NIR retrieved  $r_e$  exhibit larger differences in comparisons with the ground-retrieved value, especially for the case of the most widely used 3.7- $\mu\text{m}$  channel.

## 6. Concluding Remarks

[27] Cloud microphysical properties of droplet effective radius (DER) and liquid water path (LWP) are critically needed in climate studies because cloud microphysical processes control the conversion between water vapor, cloud droplets, and precipitation. Information on the vertical structure of cloud microphysics is fundamental in understanding the radiative effects of clouds, interactions between clouds and aerosols, hydrological implication of clouds in the earth-atmosphere system, and the important cloud-climate feedback mechanism.

[28] Conventional satellite remote sensing technique has been limited to the retrieval of a vertically invariant DER using a single near-infrared (NIR) channel, which usually does not represent the entire cloud column. In this paper, we compared a previous method presented by *Chang and Li* [2002] and two modified ones, all applicable to the Moderate-resolution Imaging Spectro-radiometer (MODIS), to retrieve three types of DER vertical profiles (DVPs) for stratiform water clouds. The three analytic DVPs were specified as linear functions of: (1) in-cloud optical depth, (2) geometric height, and (3) liquid water content (LWC) that varies linearly with height. To enhance the DVP retrievals, a split-window technique is introduced to determine the precipitable water above the cloud for correcting the water vapor attenuation in the satellite radiance measurements.

[29] As a preliminary assessment of the retrieval algorithms, the three DVP retrieval schemes were applied to the MODIS Level-1B 1-km radiance data on board the Terra satellite. Two relatively uniform cloud layers observed on April 16 and May 31, 2001 at north-central Oklahoma Southern Great Plains site were studied, where three DVPs retrieved from the MODIS satellite measurements and two DVPs retrieved from ground-based measurements were compared. The two platforms of DVP retrievals are close in magnitude and exhibit the same trends in vertical variation, attesting to the soundness and robustness of the retrieval algorithms. The different behaviors of the DER structure may be associated with different cloud development stages. Such differences may be useful for studying the aerosol indirect effects on clouds as revealed in the studies of *Rosenfeld and Lensky* [1998] and *Rosenfeld* [2000].

[30] It is also demonstrated that the modified DVP retrievals may provide more sound satellite estimates of cloud LWP. Preliminary comparisons among the three DVP schemes show that using the DVP retrieval with the assumption of LWC proportional to height appears to be superior in the LWP and DER estimates. A thorough validation study is underway for a wide range of cloud conditions. It is believed that the DVP retrievals may bear more importance not only in inferring more accurate cloud LWP, but also in observing the different stages of cloud vertical development. Since conventional DER retrievals with a single NIR channel are only sensitive to a few units in the uppermost cloud optical thickness, any DER variation within the cloud may suggest biases in cloud LWP estimates that assume a constant DER profile. Such biases can hinder the understanding of cloud processes and remote sensing analysis.

## Appendix A: Relationships Between $dr_e/d\tau$ , $dr_e/dz$ , and $d\text{LWC}/dz$

[31] The DER is defined as the ratio of the third to the second moment of the droplet size spectrum [e.g., *Hansen and Travis*, 1974], that is,

$$r_e(z) = \frac{\int \pi r^3 n(r, z) dr}{\int \pi r^2 n(r, z) dr}, \quad (\text{A1})$$

where  $z$  is the geometrical height and  $n(r, z)dr$  is the number of droplets per unit volume with radius between  $r$  and  $r + dr$  at height  $z$ . The LWC is given by

$$\text{LWC}(z) = \frac{4}{3}\rho_w \int \pi r^3 n(r, z) dr, \quad (\text{A2})$$

where  $\rho_w$  is the density of water.

[32] The optical depth is defined by

$$\tau = \int \int Q_{\text{ext}} \pi r^2 n(r, z) dr dz, \quad (\text{A3})$$

where  $Q_{\text{ext}}$  is the normalized extinction efficiency ( $\sim 2$ ). Thus, by substituting Equations (A1) and (A2) into (A3), it can be derived that

$$\tau = \frac{3Q_{\text{ext}}}{4\rho_w} \int \frac{\text{LWC}(z)}{r_e(z)} dz. \quad (\text{A4})$$

[33] By following the relation,  $\text{LWC} \propto r_e^3$  [e.g., Bower *et al.*, 1994; Martin *et al.*, 1994; Brenguier *et al.*, 2000]; that is,

$$\text{LWC}(z) = \frac{4}{3}\pi\rho_w N(z)kr_e^3(z), \quad (\text{A5})$$

where  $N(z) = \int n(r, z)dr$  and  $k$  is a constant. According to observations,  $k = \sim 0.67$  for continental stratocumulus and  $k = \sim 0.80$  for maritime stratocumulus [Pontikis and Hicks, 1992; Martin *et al.*, 1994]. In this study,  $N$  is assumed to be independent of height, then equation (A4) becomes

$$\tau = C \int r_e^2(z) dz. \quad (\text{A6})$$

where  $C = \pi N k Q_{\text{ext}}$  is a constant. By taking the derivatives,  $d\tau \sim r_e^2 dz$ , so it can be derived that for DVP1,  $dr_e/d\tau \sim dr_e/(r_e^2 dz) \sim d(r_e^{-1})/dz$ ; for DVP2,  $dr_e/dz \sim r_e^2 dr_e/d\tau \sim dr_e^3/d\tau$ ; and for DVP3,  $d\text{LWC}/dz \sim dr_e^3/dz \sim dr_e^5/d\tau$ . To express the DER profile in relation to  $\tau$ , thus,  $r_e \propto \tau$  (DVP1),  $r_e \propto \tau^{1/3}$  (DVP2), and  $r_e \propto \tau^{1/5}$  (DVP3); or in relation to  $z$ , so that  $r_e \propto z^{-1}$  (DVP1),  $r_e \propto z$  (DVP2), and  $r_e \propto z^3$  (DVP3).

[34] **Acknowledgments.** The authors express their appreciation to the useful comments from the reviewers. The authors are grateful to Goddard DAAC and the MODIS Characterization and Support Team for processing and providing MODIS level-1B data, to the Atmospheric Radiation Measurement (ARM) program sponsored by the U.S. Department of Energy (DOE) for obtaining ground measurements, to Dr. X. Dong for providing the ground retrieval data used in Figure 5, and to Drs. S. Platnick and M. King (NASA/GSFC) for helpful discussions which motivated the investigation. This research was supported by the DOE grant DE-FG02-01ER63166 under the ARM program.

## References

Berk, A., et al., *MODTRAN4 v.2.0 User's Manual, Air Force Geophys. Lab. Tech. Rep. AFGL-TR-89-0122*, 98 pp., Air Force Mat. Comm., Hanscom AFB, Mass., 1999.

Bower, K. N., T. W. Choullarton, J. Latham, J. Nelson, M. B. Baker, and J. Jensen, A parameterization of warm clouds for use in atmospheric general circulation models, *J. Atmos. Sci.*, 51, 2722–2732, 1994.

Brenguier, J.-L., H. Pawlowska, L. Schuller, R. Preusker, J. Fischer, and Y. Fouquart, Radiative properties of boundary layer clouds: Droplet

effective radius versus number concentration, *J. Atmos. Sci.*, 57, 803–821, 2000.

Chang, F.-L., and Z. Li, Estimating the vertical variation of cloud droplet effective radius using multispectral near-infrared satellite measurements, *J. Geophys. Res.*, 107, 1–12, 2002.

Chang, F.-L., Z. Li, and S. A. Ackerman, Examining the relationship between cloud and radiation quantities derived from satellite observations and model calculations, *J. Clim.*, 13, 3842–3859, 2000.

Chang, F.-L., Z. Li, and X. Dong, A bi-spectral near-infrared method for inferring the vertical variation of cloud droplet effective radius, *Proceedings of the 11th Conference on Atmospheric Radiation*, AMS, Ogden, Utah, 3–7 June 2002.

Chesters, D., L. W. Uccellini, and W. D. Robinson, Low-level water vapor fields from the VISSR Atmospheric Sounder (VAS) “split window” channels, *J. Clim. Appl. Meteorol.*, 22, 725–743, 1983.

Coakley, J. A., Jr., et al., The appearance and disappearance of ship tracks on large spatial scales, *J. Atmos. Sci.*, 57, 2765–2778, 2000.

Dong, X., and G. G. Mace, Profiles of low-level stratus cloud microphysics deduced from ground-based measurements, *J. Atmos. Oceanic Technol.*, 20, 42–53, 2003.

Frisch, A., C. W. Fairall, and J. B. Snider, Measurement of stratus cloud and drizzle parameters in ASTEX with a K-band Doppler radar and a microwave radiometer, *J. Atmos. Sci.*, 52, 2788–2799, 1995.

Guichard, F., D. Parsons, and E. Miller, Thermo-dynamic and radiative impact of the correction of sounding humidity bias in the Tropics, *J. Clim.*, 13, 3615–3624, 2000.

Han, Q., W. B. Rossow, and A. A. Lacis, Near-global survey of effective droplet radii in liquid water clouds using ISCCP data, *J. Clim.*, 7, 465–497, 1994.

Han, Q., W. B. Rossow, J. Chou, and R. M. Welch, Global survey of the relationships of cloud albedo and liquid water path with droplet size using ISCCP, *J. Clim.*, 11, 1516–1528, 1998.

Hansen, J. E., and L. D. Travis, Light scattering in planetary atmospheres, *Space Sci. Rev.*, 16, 527–610, 1974.

Harrison, E. F., P. Minnis, B. R. Barkstrom, V. Ramanathan, R. D. Cess, and G. G. Gibson, Seasonal variation of cloud radiative forcing derived from the earth radiation budget experiment, *J. Geophys. Res.*, 95, 18,687–18,703, 1990.

Hartmann, D. L., M. E. Ockert-Bell, and M. L. Michelsen, The effect of cloud type on the Earth's energy balance Global analysis, *J. Clim.*, 5, 1281–1304, 1992.

Intergovernmental Panel on Climate Change (IPCC), *Climate Change: The Scientific Basis*, edited by J. T. Houghton et al., 944 pp., Cambridge Univ. Press, New York, 2001.

Kaufman, Y. J., and T. Nakajima, Effect of Amazon smoke on cloud microphysics and albedo-Analysis from satellite imagery, *J. Appl. Meteorol.*, 32, 729–744, 1993.

King, M. D., Y. J. Kaufman, W. P. Menzel, and D. Tanre, Remote sensing of cloud, aerosol, and water vapor properties from the Moderate Resolution Imaging Spectrometer (MODIS), *IEEE Trans. Geosci. Remote Sens.*, 30, 1–27, 1992.

King, M. D., W. P. Menzel, Y. J. Kaufman, D. Tanre, B. C. Gao, S. Platnick, S. A. Ackerman, L. A. Remer, R. Pincus, and P. A. Hubanks, Cloud and aerosol properties, precipitable water, and profiles of temperature and humidity from MODIS, *IEEE Trans. Geosci. Remote Sens.*, 41, 442–458, 2003.

Kleespies, T. J., and L. M. McMillin, Physical retrieval of precipitable water using the split window technique, *Preprints Conference on Satellite Meteorology/Remote Sensing and Applications*, pp. 55–57, AMS, Boston, Mass., 1984.

Liljgren, J. C., E. E. Clothiaux, G. G. Mace, S. Kato, and X. Dong, A new retrieval for cloud liquid water path using a ground-based microwave radiometer, and measurements of cloud temperature, *J. Geophys. Res.*, 106, 14,485–14,500, 2001.

Martin, G. M., D. W. Johnson, and A. Spice, The measurement and parameterization of effective radius of droplets in warm stratocumulus clouds, *J. Atmos. Sci.*, 51, 1823–1842, 1994.

Miles, N. L., J. Verlinde, and E. E. Clothiaux, Cloud droplet size distributions in low-level stratiform clouds, *J. Atmos. Sci.*, 57, 295–311, 2000.

Nakajima, T. Y., and T. Nakajima, Wide-area determination of cloud microphysical properties from NOAA AVHRR measurements for FIRE and ASTEX regions, *J. Atmos. Sci.*, 52, 4043–4059, 1995.

Pilewskie, P., and S. Twomey, Cloud phase discrimination by reflectance measurements near 1.6 and 2.2  $\mu\text{m}$ , *J. Atmos. Sci.*, 44, 3419–3420, 1987.

Platnick, S., Vertical photon transport in cloud remote sensing problems, *J. Geophys. Res.*, 105, 22,919–22,935, 2000.

Platnick, S., and S. Twomey, Determining the susceptibility of cloud albedo to changes in droplet concentrations with the Advanced

- Very High Resolution Radiometer, *J. Appl. Meteorol.*, 33, 334–347, 1994.
- Platnick, S., M. D. King, S. A. Ackerman, W. P. Menzel, B. A. Baum, J. C. Riedi, and R. A. Frey, The MODIS cloud products: Algorithms and examples from Terra, *IEEE Trans. Geosci. Remote Sens.*, 41, 459–473, 2003.
- Pontikis, C. A., and E. Hicks, Contribution to the cloud droplet effective radius parameterization, *Geophys. Res. Lett.*, 19, 2227–2230, 1992.
- Rosenfeld, D., Suppression of rain and snow by urban and industrial air pollution, *Science*, 287, 1793–1796, 2000.
- Rosenfeld, D., and M. I. Lensky, Space-borne based insights into precipitation formation processes in continental and maritime convective clouds, *Bull. Am. Meteorol. Soc.*, 79, 2457–2476, 1998.
- Stephens, G. L., Radiation profiles in extended water clouds. II: Parameterization schemes, *J. Atmos. Sci.*, 35, 2123–2132, 1978.
- Stephens, G. L., Radiative effects of clouds and water vapor, in *Global Energy and Water Cycle*, edited by K. A. Browning and R. J. Gurney, pp. 71–90, Cambridge Univ. Press, New York, 1999.
- Szczodrak, M., P. H. Austin, and P. B. Krummel, Variability of optical depth and effective radius in marine stratocumulus clouds, *J. Atmos. Sci.*, 58, 2912–2926, 2001.
- Turner, D. D., B. M. Lesht, S. A. Clough, J. C. Liljegren, H. E. Revercomb, and D. C. Tobin, Dry bias and variability in Vaisala RS80–H radiosondes: The ARM experience, *J. Atmos. Oceanic Technol.*, 20, 117–132, 2003.

---

F.-L. Chang and Z. Li, Earth System Science Interdisciplinary Center, 2207 Computer and Space Sciences Bldg, University of Maryland, College Park, MD 20742, USA. (fchang@essic.umd.edu)